A MULTISCALE APPROACH FOR PARTICLE TRANSPORT SIMULATION IN LOW REYNOLDS NUMBER FLOWS

DENIS JAREMA , PHILIPP NEUMANN , AND TOBIAS WEINZIERL *

Abstract. In this paper, we study a nanoparticle suspended in water within a channel with a complex wall geometry in a laminar flow regime. We combine two independent iterative methods into one multiscale approach to compute the movement of the particle: a Lattice Boltzmann fluid-structure interaction code and a Navier-Stokes solver with the Faxén particle force estimation. A new switching strategy between these two methods is developed. On the one hand, the computationally expensive Lattice Boltzmann fluid-structure code is used in time intervals when short-time effects may yield a strong impact on the particle simulation. On the other hand, the Navier-Stokes solver with the Faxén correction is used to compute the particle movement when long-time predictions to the particle motion are possible and sufficient. We describe our coupling strategy, the mapping of unknowns between the two solvers and provide results for different particulate flow scenarios. Due to coupling of the two systems and the automatic switching we reduce the total computing time by magnitudes.

1. Introduction. Particle transport phenomena are of interest in industry and science. Motion of nanoparticles in blood attracts a considerable attention in pharmacology [6], and in the environmental sciences it is important to determine the location of contaminant sediments [17]. Other interesting examples include hydrodynamic Brownian motors or drift ratchets [9, 14]. The latter microscopic device type has proven to be very efficient for sorting molecules depending on their size and weight.

Referring to the simulation of the underlying process, a fluid-structure interaction (FSI) problem needs to be solved. However, not all experiments require the full model to trace the particles accurately. If fluid flow is laminar, if the particle is far away from outer boundaries, and if there is no particle-particle interplay, a unidirectional coupling neglecting the influence of the particle on the flow yields already accurate results [20]. Several approaches exist which allow to compute the hydrodynamic force for compressible and incompressible fluids, different flow types, and different shapes of particles in such simplified settings [3, 8, 13, 15, 16, 18, 23]. Amongst others, Faxén theorems [5] provide means to compute translational and rotational hydrodynamic forces acting on a particle in the Stokes flow regime.

There are relevant effects of interest such as particle drifts [2] that require simulation runs tackling long time intervals and capturing physical transport phenomena on different time scales. We focus on laminar flows with one particle, and we propose an iterative procedure of switching back and forth between two different flow solvers. One FSI solver addresses settings where the Faxén theorem cannot be applied owing to complicated domain shapes that affect the motion of the particles. Due to the long time scale involved, it is, however, not possible to compute the underlying problem by the FSI code all alone. It is computationally too expensive as it requires an accurate spatial resolution, and the interaction imposes severe constraints on the biggest timestep size that may be chosen. While FSI yields accurate results for all settings, the particle nevertheless may spend considerable time far away from any wall. Therefore, we propose to combine the two approaches, full FSI and the Faxén method, and to switch to the appropriate model depending on the current situation. The force postprocessing computations required by Faxén approach are fast and allow big time steps; the FSI method is precise (Figure 1.1).

* Scientific Computing in Computer Science, Technische Universität München, Boltzmannstraße 3, 85748 Garching, Germany ({jarema,neumanph,weinzier}@in.tum.de).

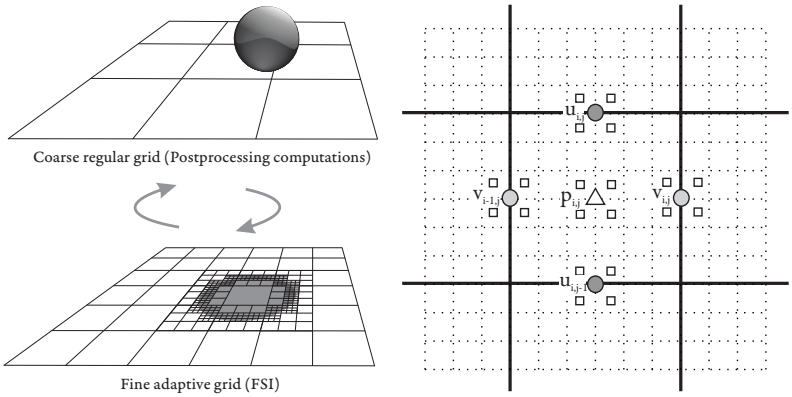

FIGURE 1.1. *Left: two different simulation modes: Faxén postprocessing can be applied on a coarse grid using big timesteps (top) whereas the particle motion can be solved by full FSI using finer grids and timesteps (bottom). Right: bilinear interpolation of Navier-Stokes equations quantities on a staggered grid from the Lattice-Boltzmann values. Only four values in the small squares are required for each interpolation.*

Choosing the appropriate method – FSI or Faxén – requires a detection system that automatically decides when to switch between the methods. In the present paper, we propose to switch when the particle is close to walls or the flow field around the particle shows severe changes over time. Our FSI code is based on the Lattice-Boltzmann method and a simple spherical particle model, as its mesoscale description allows precise computations of forces [10, 11] and the incorporation of thermal fluctuations [4]. Furthermore, Lattice-Boltzmann codes are known to fit well to massively parallel supercomputers. For the Faxén force computations we apply a finite difference solver of the Navier-Stokes equations. It uses explicit timestepping. For the Navier-Stokes equations solver, we further use a significantly coarser grid than for the Lattice-Boltzmann method (Figure 1.1). Besides, during the Navier-Stokes equations simulations we do not refine the grid near the particle. The resulting grid is thus regular and a good starting point to use geometric or geometrically inspired multigrid solvers such as [24] for the underlying pressure Poisson equations.

The idea presented in the paper is motivated by the drift ratchet device from [9]. In [19], the author proposes to study exclusively the postprocessing forces for such a setting, and he uses the Faxén theorems to compute the hydrodynamic interaction forces and a Langevin description for the involved Brownian motion. Without a quantification, he states that this model is not accurate in general. A full FSI model for the drift ratchet on the other hand is elaborated in [2]. According to this work, even today's supercomputers are far from able to resolve this problem on long time scales with reasonable spatial resolutions. We hence combine these two approaches to improve performance of simulations without a significant loss of accuracy.

The remainder of this paper is organized as follows: In Section 2, we provide a detailed description of the two numerical methods that we use in our simulations. The coupling of the two particle transport methods is introduced in Section 3. We compare the forces obtained from the two approaches and present results of the drift ratchet simulations in Section 4. A short outlook and recapitulation close the discussion in Section 5.

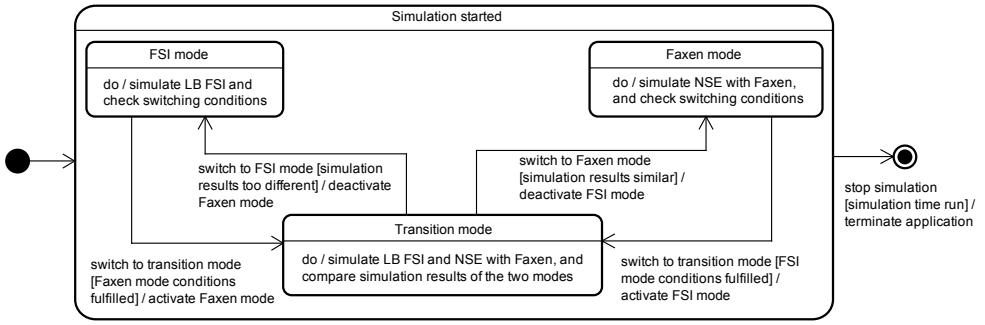

FIGURE 2.1. *Particle transport simulation state diagram. The Faxén mode is running with big timesteps on a coarse grid, and the FSI mode is running with small timesteps on a finer grid.*

2. Two fluid-particle interaction models. In this paper, we start from regular Cartesian grid representing the computational domain without any particle. Into this Cartesian grid, we embed a second adaptive Cartesian grid resolving the particle. Each coarse grid point also is a fine grid point besides those interfering with the particle (Figure 1.1). This notion of embedded grids follows [21, 22] and both fluid codes rely on the same data structures. On the coarse grid, we realize a simple Navier-Stokes solver with a totally staggered degree of freedom layout and explicit time stepping [7]. On top of this solver, we implement Faxén's description discussed on the following pages, while, on the fine grid, we realize a Lattice-Boltzmann FSI code. As the Faxén description is not accurate if the particle is close to the walls or the flow field around the particle is undergoing strong temporal changes, we propose to use an expert system which decides when to switch and which simulation to run.

From the derivation in [19] of the Faxén theorems, we know that it is difficult to estimate good thresholds, such as the distance of the particle from the wall and the dynamic behavior of the fluid flow, which are required for the switching process. For that reason, during switching, we run the two models simultaneously for a given time interval $\Delta t^{(\mathrm{FSI,Faxen})}$. Then we compare the particle positions of the FSI code $\mathbf{X}^{(\mathrm{FSI})}$ with the one of the Faxén approach $\mathbf{X}^{(\mathrm{Faxen})}$. If they differ significantly, i.e. $\|\mathbf{X}^{(\mathrm{FSI})} - \mathbf{X}^{(\mathrm{Faxen})}\| > \varepsilon^{(\mathrm{FSI,Faxen})}$, we continue with the FSI code only for a given time interval $\Delta t^{(\mathrm{FSI})}$ before we compare again. If they do not differ significantly, we continue with the Faxén code until a given time span $\Delta t^{(\mathrm{Faxen})}$ has passed, or until the particle approaches the wall, or until the difference of the particle speed compared to the virtually surrounding flow exceeds a given threshold $\varepsilon^{(\mathrm{Faxen})}$ (Figure 2.1).

2.1. Lattice-Boltzmann Method. The Lattice-Boltzmann method delivers a mesoscopic description of the physical properties and, hence, is well suited for nano- and microscale simulations. The method we use is based on a discretization of the Boltzmann equation on a cubic lattice. The time evolution of the distribution functions $f_k(\mathbf{r}, t)$, which describe the probabilities to find molecules within the center point of a lattice cell $\mathbf{r}$ at time t, consists of two main steps. We start with a collision step which models molecular interactions on the statistical mesoscale:

$$f'_k(\mathbf{r}, t) = f_k(\mathbf{r}, t) + \Delta_k \left(f(\mathbf{r}, t) - f^{(eq)}(\mathbf{r}, t) \right), \tag{2.1}$$

where $f'_k(\mathbf{r}, t)$ is the distribution function after collision, Δ_k is the collision operator, and $f^{(eq)}(\mathbf{r}, t)$ is the discrete Maxwell-Boltzmann equilibrium distribution function.

The operator Δ_k is approximated by the Bhatnagar-Gross-Krook (BGK) [1] or the multiple relaxation time scheme from [4] incorporating Brownian effects. After the collision step, the distributions are propagated to the neighboring cells according to

$$f_k(\mathbf{r} + \delta t \mathbf{v}_k, t + \delta t) = f'_k(\mathbf{r}, t), \tag{2.2}$$

modeling the convective behavior of the system. During this step, the molecules move to the neighboring cells at discrete velocities $\mathbf{v}_k$.

The computation of the force acting on a spherical particle in the Lattice-Boltzmann FSI code is based on the momentum exchange method [10, 11, 25]. The total force acting on the particle is given by

$$\mathbf{W}^{(\mathrm{FSI})} = \sum_{x_f} \sum_{k} \mathbf{v}_{\mathrm{inv}(k)} \left[f_{\mathrm{inv}(k)}(x_f) + f_k(x_b) \right], \qquad \mathbf{v}_{\mathrm{inv}(k)} = -\mathbf{v}_k, \tag{2.3}$$

where the outer sum is taken over all fluid cells near the moving sphere, and the inner sum involves all velocity directions $\mathbf{v}_k$ that connect the boundary cell x_b with the fluid cell x_f.

After evaluating the force, we update the particle position $\mathbf{X}^{(\mathrm{FSI})}$ and velocity $\mathbf{V}^{(\mathrm{FSI})}$ using a staggered explicit timestepping scheme:

$$\begin{aligned} \mathbf{V}^{(\mathrm{FSI})}(t + \tfrac{1}{2}\,\mathrm{d}t) &= \mathbf{V}^{(\mathrm{FSI})}(t - \tfrac{1}{2}\,\mathrm{d}t) + \tfrac{\mathrm{d}t}{m_p} \mathbf{W}^{(\mathrm{FSI})}(t), \\ \mathbf{X}^{(\mathrm{FSI})}(t + \mathrm{d}t) &= \mathbf{X}^{(\mathrm{FSI})}(t) + \tfrac{1}{2} \left[\mathrm{d}t \mathbf{V}^{(\mathrm{FSI})}(t - \tfrac{1}{2}\,\mathrm{d}t) + \mathbf{V}^{(\mathrm{FSI})}(t + \tfrac{1}{2}\,\mathrm{d}t) \right]. \end{aligned} \tag{2.4}$$

Based on the new position, the obstacle and fluid cells are reflagged and initialized correspondingly. The whole scheme is implemented on top of an adaptive Cartesian grid.

2.2. Navier-Stokes Equations with Faxén Correction. If we decide that the Faxén approach is accurate enough, we solve the Navier-Stokes equations for an incompressible flow:

$$\begin{aligned} &\frac{\partial \mathbf{u}}{\partial t} + (\mathbf{u} \cdot \nabla)\,\mathbf{u} = -\nabla p + \frac{1}{\mathrm{Re}} \Delta \mathbf{u} + \mathbf{F}, \\ &\nabla \cdot \mathbf{u} = 0, \end{aligned} \tag{2.5}$$

where $\mathbf{u}$ is the fluid velocity, p the pressure, Re the Reynolds number, and $\mathbf{F}$ an external volume force. The first set of equations corresponds to the law of momentum conservation, the last equation represents mass conservation.

We apply the predictor-corrector scheme to solve the equations on a regular Cartesian grid [7]. From given fluid velocities $\mathbf{u}(t)$ at timestep t we predict a fluid velocity for the new timestep $t + 1$. Then we compute the pressure at $t + 1$ from a Poisson equation that arises from the assumption of mass conservation and the predicted velocities $\mathbf{u}(t + 1)$. The predicted velocities are corrected using the new pressure values at $t + 1$.

The forces acting on a suspended particle are computed in a postprocessing step at the end of each timestep. They stem from Faxén theorems [5] and read

$$\mathbf{W}^{(\mathrm{Faxen})}_{(\mathrm{2D})} = \frac{4\pi\eta l}{\ln(l/a)} \left(\mathbf{u} - \mathbf{V}^{(\mathrm{Faxen})} \right) + \frac{\pi \eta l a^2}{\ln(l/a)} \boldsymbol{\nabla}^2 \cdot \mathbf{u}, \tag{2.6}$$

$$\mathbf{W}^{(\mathrm{Faxen})}_{(\mathrm{3D})} = 6\pi\eta a (\mathbf{u} - \mathbf{V}^{(\mathrm{Faxen})}) + \pi \eta a^3 \boldsymbol{\nabla}^2 \cdot \mathbf{u}, \tag{2.7}$$

where $\mathbf{W}_{(2D)}^{(\text{Faxen})}$ is the force acting on a cylindrical particle of length l and radius a, and $\mathbf{W}_{(3D)}^{(\text{Faxen})}$ is the force acting on a spherical particle of radius a. In both formulas, $\mathbf{V}^{(\text{Faxen})}$ is the velocity of the particle and $\mathbf{u}$ is the fluid velocity in the center of the particle.

The new particle position $\mathbf{X}^{(\text{Faxen})}$ and velocity $\mathbf{V}^{(\text{Faxen})}$ are computed in each timestep from semi-explicit Euler updates for Newton's laws of motion:

$$\begin{aligned} \mathbf{V}^{(\text{Faxen})}(t+\mathrm{d}t) &= \mathbf{V}^{(\text{Faxen})}(t) + \tfrac{\mathrm{d}t}{m_p}\mathbf{W}^{(\text{Faxen})}(t), \\ \mathbf{X}^{(\text{Faxen})}(t+\mathrm{d}t) &= \mathbf{X}^{(\text{Faxen})}(t) + \mathrm{d}t\mathbf{V}^{(\text{Faxen})}(t+\mathrm{d}t). \end{aligned} \tag{2.8}$$

The particle here is not associated with an obstacle. It does not influence the fluid.

3. Coupling between Lattice-Boltzmann and Navier-Stokes solvers. Our overall simulation is a time stepping algorithm built on top of an iterative solver for the pressure equation. Transitions

$$\begin{aligned} \mathcal{P}_{(\text{Faxen})}^{(\text{FSI})} &: \{f_k, \mathbf{X}^{(\text{FSI})}, \mathbf{V}^{(\text{FSI})}\} \mapsto \{\mathbf{u}, p, \mathbf{X}^{(\text{Faxen})}, \mathbf{V}^{(\text{Faxen})}\}, \\ \mathcal{P}_{(\text{FSI})}^{(\text{Faxen})} &: \{\mathbf{u}, p, \mathbf{X}^{(\text{Faxen})}, \mathbf{V}^{(\text{Faxen})}\} \mapsto \{f_k, \mathbf{X}^{(\text{FSI})}, \mathbf{V}^{(\text{FSI})}\}, \end{aligned} \tag{3.1}$$

are required in order to switch from the Faxén to the FSI approach and vice versa.

3.1. Transition to the Faxén approach. We distinguish two types of transitions: one for the fluid $\{f_k\} \mapsto \{\mathbf{u}, p\}$ and another for the particle $\{\mathbf{X}^{(\text{FSI})}, \mathbf{V}^{(\text{FSI})}\} \mapsto \{\mathbf{X}^{(\text{Faxen})}, \mathbf{V}^{(\text{Faxen})}\}$.

With $\mathcal{P}_{(\text{FSI})}^{(\text{Faxen})}$, the transition for the particle corresponds to the scaling to the dimensionless units of the Navier-Stokes equations

$$\mathbf{X}^{(\text{Faxen})} = \mathbf{X}^{(\text{FSI})} \quad \text{and} \quad \mathbf{V}^{(\text{Faxen})} = \mathbf{V}^{(\text{FSI})}/\tilde{u}, \tag{3.2}$$

where $\tilde{u}$ is the characteristic fluid velocity (in a channel flow, for example, its value corresponds to the fluid velocity at the inlet). For the transition $\mathcal{P}_{(\text{FSI})}^{(\text{Faxen})}$, we use the inverse of the last equation.

During the transition for the fluid, we estimate macroscopic quantities (velocity and pressure) at each grid point from the probability distribution functions:

$$p^{(\text{LB})} = \rho^{(\text{LB})} c_s^2 = c_s^2 \sum_{k=1}^{Q} f_k, \qquad \rho\mathbf{u}^{(\text{LB})} = \sum_{k=1}^{Q} f_k \mathbf{v}_k, \tag{3.3}$$

where $p^{(\text{LB})}$, $\rho^{(\text{LB})}$, and $\mathbf{u}^{(\text{LB})}$ are the dimensionless LB pressure, density and velocity; $c_s := \frac{1}{\sqrt{3}}$ is the dimensionless speed of sound on the lattice. The dimensional quantities are given by

$$\mathbf{u} = \mathbf{u}^{(\text{LB})} \frac{\mathrm{d}x}{\mathrm{d}t}, \qquad p = p^{(\text{LB})} \cdot \rho \cdot \frac{\mathrm{d}x^2}{\mathrm{d}t^2}, \tag{3.4}$$

where $\mathrm{d}x$ and $\mathrm{d}t$ are the mesh size and timestep of the LB simulation and ρ the density of the fluid. Next, we rescale these quantities to the dimensionless NSE, see amongst others [7].

We run the Lattice-Boltzmann code on a finer grid than the Navier-Stokes equations solver. Therefore, to estimate the macroscopic parameters we use only the

Lattice-Boltzmann cells adjacent to the pressure and velocity nodes of the staggered Navier-Stokes grid (Figure 1.1).

In the FSI mode, the particle is represented by a spherical obstacle, but in the Faxén mode, it is virtual. Consequently, during $\mathcal{P}^{(\mathrm{FSI})}_{(\mathrm{Faxen})}$, we do not have the fluid velocities specified in the cells that are located within the particle geometry. In these locations, we assign the particle velocity and zero pressure to the fluid. The correct pressure is recovered when solving the first pressure Poisson equation.

Due to the differences between the flow models, the fluid flow carries undesired perturbations after switching. Therefore, we do not run simulations immediately after the transition. Instead, we fix the particle, stop time counters and let the system recover over several iterations.

3.2. Transition to the FSI mode. There is no unique way for $\mathcal{P}^{(\mathrm{Faxen})}_{(\mathrm{FSI})}$, because the degrees of freedom of the Navier-Stokes system – i.e. the pressure and velocity values – do not provide enough information for the statistical mesoscale description of the LB approach. Furthermore, we have to recover values on the finer grid from the coarse one (in all experiments described in the paper, the LB grid resolution is six times finer than the NSE grid).

During $\mathcal{P}^{(\mathrm{Faxen})}_{(\mathrm{FSI})}$, we interpolate the fluid velocities and pressures in each Lattice-Boltzmann cell center. Afterwards, we apply inverse functions of (3.4) to obtain the dimensionless quantities on the Lattice-Boltzmann grid. However, the pressure in the Navier-Stokes equations may vary by a constant offset. Therefore, before converting the pressure to the Lattice-Boltzmann units, we shift the pressure according to [12]:

$$\rho^{(\mathrm{LB})} = \rho \left[\frac{p}{c_s^2} - \left\langle \frac{p}{c_s^2} \right\rangle + 1 \right], \tag{3.5}$$

where $\langle \ldots \rangle$ denotes the average value over all LB cells.

From the macroscopic velocities and densities in the LB cells, we determine the distribution functions. In our application, we recover the equilibrium part of the distribution function $f_k^{(eq)}$ from the macroscopic quantities.

As in the transition case $\mathcal{P}^{(\mathrm{FSI})}_{(\mathrm{Faxen})}$, we need to eliminate perturbations caused by switching during a recovery period in the LB simulation where the boundary conditions are fixed and a steady state is assumed.

4. Simulation Results.

4.1. Transition Analysis. The number of iterations of Gauss-Seidel (GS) type solvers necessary to remove pollution effects due to $\mathcal{P}^{(\mathrm{FSI})}_{(\mathrm{Faxen})}$ can be estimated from Figure 4.1. In these experiments, we used a two-dimensional channel scenario. The number of timesteps does not strongly depend on the Reynolds number for the regimes under consideration. It is only five to six steps for the GS solver and three to four timesteps for the SOR solver that are sufficient to reach steady state, demonstrating the efficiency of our switching from the LB to the NSE solver.

To analyze the transition process from perturbed to steady perturbation-reduced flow after $\mathcal{P}^{(\mathrm{Faxen})}_{(\mathrm{FSI})}$, we compute the average change of the fluid density between two subsequent LB iterations:

$$\Delta\rho = \frac{1}{N} \left[\sum_{i=1}^{N} \left(\rho_i^{(new)} - \rho_i^{(old)} \right)^2 \right]^{\frac{1}{2}}, \tag{4.1}$$

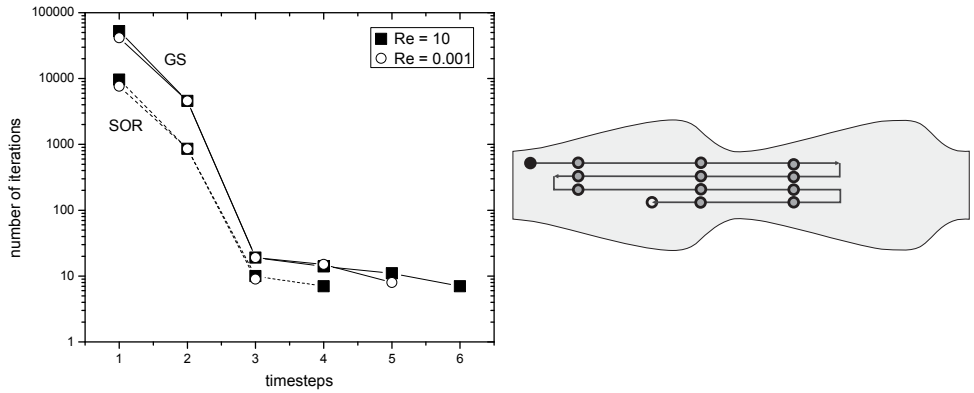

FIGURE 4.1. *Left: Number of the Gauss-Seidel (GS) and successive over-relaxation (SOR) solvers iterations after switching from the LB to NSE simulations. Right: Schematic representation of the particle trajectory. Particle is moving in the center along the channel axis. The switching occurs approximately in the gray circles.*

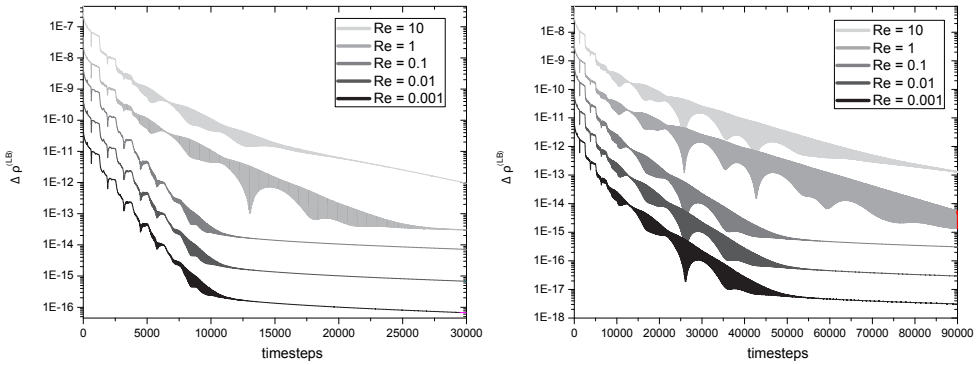

FIGURE 4.2. *Density change over time in a LB simulation. The results are shown for LB grids of size* 360×72 *(left) and* 720×144 *(right).*

where we take the sum over all LB fluid cells. In Figure 4.2 we provide plots of the average density change $\Delta\rho$ depending on the number of timesteps. During the transition process, the density change decays exponentially over time.

4.2. Comparison of Forces. To investigate the range of applicability of Faxén theorems, we compare the postprocessing forces acting on a particle with the ones obtained from the full FSI simulations.

In our experiments, we use a channel scenario and initially fix the particle in the center of the channel. We let the fluid flow stabilize and then release the particle. The particle is accelerated by the surrounding flow until it reaches a constant velocity. During the transition process, we measure force dependencies on the particle velocity.

The flow field for the two-dimensional channel is described via

$$\frac{\partial p}{\partial x} = -\mathrm{G}, \quad \text{and} \quad u(y) = \frac{1}{2} \cdot \mathrm{Re} \cdot \mathrm{G} \cdot y(d-y), \tag{4.2}$$

where d is the distance between the walls or the diameter of the tube. However, for three dimensions the formula is multiplied by factor $1/4$ instead of $1/2$.

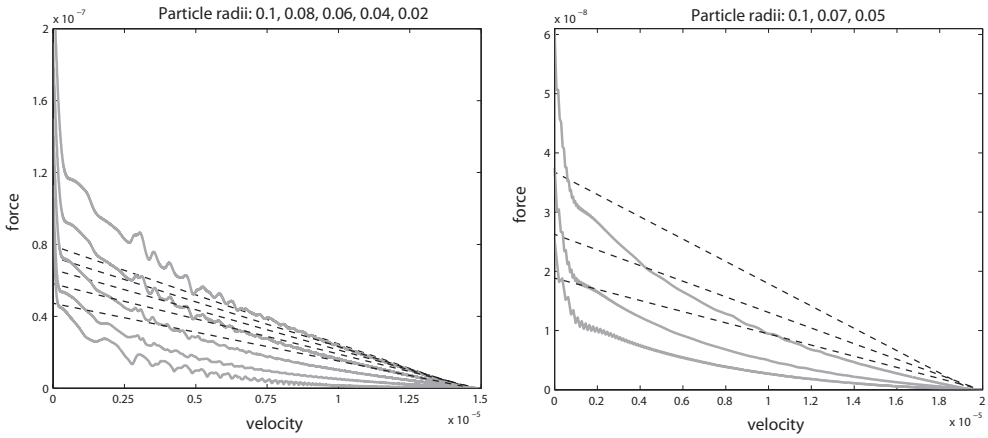

FIGURE 4.3. *Force dependencies on the particles velocity for the two- (left plot) and three-dimensional (right plot) channels. The gray solid lines correspond to simulation measurements, the dashed black lines are Faxén forces. The force is decreasing by reducing the radius of the particle.*

If we directly apply (2.6) and (2.7) correspondingly to the two- and three-dimensional channels, we obtain the analytical expressions for the Faxén forces:

$$\mathrm{W}_{(\mathrm{2D})}^{(\mathrm{NSE})} = \frac{4\pi\eta l}{\ln\left(l/a\right)}\left[\left(u - \frac{1}{4}a^2 \cdot \mathrm{Re} \cdot \mathrm{G}\right) - V\right], \tag{4.3}$$

$$\mathrm{W}_{(\mathrm{3D})}^{(\mathrm{NSE})} = 6\pi\eta a\left[\left(u - \frac{1}{12}a^2 \cdot \mathrm{Re} \cdot \mathrm{G}\right) - V\right]. \tag{4.4}$$

We compare these linear dependencies on the particle velocity with the results from the full FSI simulations using particles with density $\rho = 2.0$ and a characteristic velocity $u_c = 0.00001$ at the channel inlet. We provide measurements results for the two-dimensional and three-dimensional channels with particles of different radii in Figure 4.3.

The difference between the FSI and Faxén force is due to the inertia force term, which is neglected in the Faxén theorems. There are alternative force postprocessing formulas for tiny particles that take the missing terms into consideration [23].

4.3. Drift Ratchet Simulations. We conducted an experiment with the drift ratchet to get an insight into the performance gain due to the expert system. The particle trajectory during the simulations is schematically demonstrated in Figure 4.1.

The evolution of the simulation is demonstrated in Figure 4.4. In the plot, there are four different simulation states: FSI, Faxén, and transitions from FSI to Faxén mode and back. The slope of the line corresponds to the speed of the simulations, i.e. the ratio of elapsed simulation time to simulated time. In the case of the FSI simulations, the speed is 0.24, for the simulations with Faxén forces computation 2.5, and for the whole application 0.57. From these results, we notice that our simulation is accelerated by $0.57/0.24 \approx 2.36$ in comparison to the pure FSI interactions run. During the Navier-Stokes simulation, we speed up the application by $2.5/0.24 \approx 10.42$. The gain in performance is basically due to the coarser resolution in the Navier-Stokes case, compared to the fine grid in the Lattice-Boltzmann simulations.

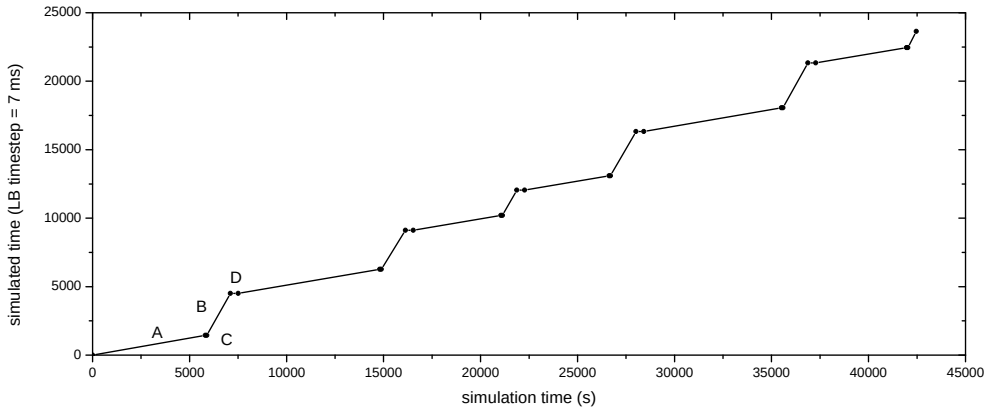

FIGURE 4.4. *Simulated time dependence on simulation or wall time; A – FSI mode, B – Faxén mode, C and D – transition from FSI to Faxén mode and back.*

5. Conclusion. An efficient multiscale approach to simulate a particle transport scenario with low Reynolds numbers has been developed. We show that the simulation running under control of an expert system outperforms a classical FSI approach if the Faxén postprocessing force computations are accurate enough, while the choice of a proper model (either full FSI or the simplified setting) is hidden in a black-box algorithm. The approach promises to help to overcome both the accuracy and runtime problems reported in [2, 19].

Future work comprises to replace the simple Gauss-Seidel type solvers used for the Navier-Stokes equations by a geometric multigrid solver [24]. Also, the parallel performance of the presented methodology has to be studied in particular with respect to load balancing issues tied to the multiscale formulation. For both endeavors, it will prove to be an advantage that all implementation components already are implemented within one computational framework [21, 22].

Finally, both this methodology, extensions of the present work, and improvements of the individual ingredients such as adaptive mesh refinement for the Lattice-Boltzmann FSI code have to lead to new scientific insight about the particle movements on the long time term. So far, our approach has been tested only for relatively short time periods and coarse grids.

Acknowledgements. Computing resources for the present work have been provided by the Gauss Centre for Supercomputing/Leibniz Supercomputing Centre under grant pr63no and grant grant pr23bu, as well as the KAUST Supercomputing Laboratory supported by Award No. UK-c0020, made by the King Abdullah University of Science and Technology (KAUST).

REFERENCES

[1] P.L. Bhatnagar, E.P. Gross, and M. Krook. A model for collision processes in gases. I. Small amplitude processes in charged and neutral one-component systems. *Phys. Rev.*, 94(3):511–525, 1954.

[2] M. Brenk, H. J. Bungartz, M. Mehl, I. L. Muntean, T. Neckel, and T. Weinzierl. Numerical simulations of particle transport in a drift ratchet. *SIAM J. Sci. Comput.*, 30(6):2777–2798, 2008.

[3] S. B. Chen and X. Ye. Faxen's laws of a composite sphere under creeping flow conditions. *Journal of Colloid and Interface Science*, 221(1):50–57, 2000.

[4] B. Dünweg, U. D. Schiller, and A. J. C. Ladd. Statistical mechanics of the fluctuating lattice Boltzmann equation. *Physical Review E*, 76, 2007.

[5] H. Faxen. *Einwirkung der Gefässwände auf den Widerstand gegen die Bewegung einer kleinen Kugel in einer zähen Flüssigkeit.* PhD thesis, Philosophische Fakultät in Uppsala, Uppsala, 1921.

[6] K. Gao and X. Jiang. Influence of particle size on transport of methotrexate across blood brain barrier by polysorbate 80-coated polybutylcyanoacrylate nanoparticles. *International Journal of Pharmaceutics*, 310:213–219, 2006.

[7] M. Griebel, T. Dornseifer, and T. Neunhoeffer. *Numerical Simulation in Fluid Dynamics. A Practical Introduction.* SIAM, Philadelphia, 1997.

[8] Y. Kaneda. A ganeralization of Faxén's theorem to nonsteady motion of an almost spherical drop in an arbitrary flow of a compressible fluid. *Physica A: Statistical and Theoretical Physics*, 101(2-3):407–422, 1980.

[9] C. Kettner, P. Reimann, P. Hänggi, and F. Müller. Drift ratchet. *Physical Review E*, 61(1):312–323, 2000.

[10] A. J. C. Ladd. Numerical simulations of particulate suspensions via a discretized Boltzmann equation. Part 1. Theoretical foundation. *Journal of Fluid Mechanics*, 271:285–309, 1994.

[11] A. J. C. Ladd. Numerical simulations of particulate suspensions via a discretized Boltzmann equation. Part 2. Numerical results. *Journal of Fluid Mechanics*, 271:311–339, 1994.

[12] J. Latt, B. Chopard, and P. Albuquerque. Spatial coupling of a Lattice Boltzmann fluid model with a finite difference Navier-Stokes solver, 2008.

[13] E. R. Lindgren. The motion of a sphere in an incompressible viscous fluid at Reynolds numbers considerably less than one. *Physica Scripta*, 60(2):97–110, 1999.

[14] S. Matthias and F. Müller. Asymmetric pores in a silicon membrane acting as massively parallel Brownian ratchets. *Letters to Nature*, 424:53–57, 2003.

[15] P. Mazur and D. Bedeaux. A generalization of Faxén's theorem to nonsteady motion of a sphere through a compressible fluid in arbitrary flow. *Physica*, 78(3):505–515, 1974.

[16] P. Mazur and D. Bedeaux. A generalization of Faxén's theorem to nonsteady motion of a sphere through an incompressible fluid in arbitrary flow. *Physica*, 76(2):235–246, 1974.

[17] P. McLaren, W. J. Cretney, and R. I. Powys. Sediment pathways in a British Columbia fjord and their relationship with particle-associated contaminants. *Journal of Coastal Research*, 9(4):1026–1043, 1993.

[18] D. Sahoo and M. C. Valsakumar. Faxen's theorem for nonsteady motion of a sphere through a fluid with internal rotation. *Physica A: Statistical and Theoretical Physics*, 196(3):349–362, 1993.

[19] M. Schindler. *Free-Surface Microflows and Particle Transport.* PhD thesis, Mathematisch-Naturwissenschaftlichen Fakultät der Universität Augsburg, Augsburg, 2006.

[20] M. Schindler, P. Talknera, M. Kostura, and P. Hänggi. Accumulating particles at the boundaries of a laminar flow. *Physica A: Statistical Mechanics and its Applications*, Volume 385(1):46–58, 2007.

[21] T. Weinzierl. *A Framework for Parallel PDE Solvers on Multiscale Adaptive Cartesian Grids.* Dissertation, Institut für Informatik, Technische Universität München, München, 2009.

[22] T. Weinzierl and M. Mehl. Peano – a traversal and storage scheme for octree-like adaptive cartesian multiscale grids. *SIAM Journal on Scientific Computing*, 33(5):2732–2760, October 2011.

[23] A. J. Weisenborn and P. Mazur. The Oseen drag on a circular cylinder revisited. *Physica A: Statistical and Theoretical Physics*, 123(1):191–208, 1984.

[24] I. Yavneh and M. Weinzierl. Nonsymmetric black box multigrid with coarsening by three. *Numerical Linear Algebra with Applications, Special Issue Copper Mountain 2011*, 2012. accepted.

[25] D. Yua, R. Meia, L. S. Luob, and W. Shyya. Viscous flow computations with the method of lattice Boltzmann equation. *Progress in Aerospace Sciences*, 39:329–367, 2003.